

High-order dispersion suppression for FFAG-based optics

This article has been downloaded from IOPscience. Please scroll down to see the full text article.

2012 JINST 7 P05011

(<http://iopscience.iop.org/1748-0221/7/05/P05011>)

View [the table of contents for this issue](#), or go to the [journal homepage](#) for more

Download details:

IP Address: 130.246.132.178

The article was downloaded on 01/06/2012 at 16:51

Please note that [terms and conditions apply](#).

High-order dispersion suppression for FFAG-based optics

R. Fenning,^{a,1} S. Machida,^b D. Kelliher,^b A. Khan^a and R. Edgecock^c

^a*Brunel University,*

Uxbridge, Middlesex, UB8 3PH United Kingdom

^b*ASTeC, STFC Rutherford Appleton Laboratory,*

Harwell Science and Innovation Campus, Didcot, OX11 0QX, United Kingdom

^c*Particle Physics Department, STFC Rutherford Appleton Laboratory,*

Harwell Science and Innovation Campus, Didcot, OX11 0QX, United Kingdom

E-mail: richardfenning@yahoo.co.uk

ABSTRACT: The resurgence of interest in FFAG type magnets has motivated the desire for high-order dispersion suppression to aid the development of dispersion-free straight sections to currently circular designs. In scaling FFAGs, dispersion suppression can only be achieved over a limited momentum range and breaks down as high-order chromatic aberration terms become significant. However by breaking the scaling law and varying the individual multipole components, these can be compensated for and a design for high-order dispersion suppression achieved. This paper presents a process for doing so and discusses the impact on beta functions, as well as the effect of magnet positioning errors.

KEYWORDS: Accelerator modelling and simulations (multi-particle dynamics; single-particle dynamics); Beam Optics; Beam dynamics; Accelerator Subsystems and Technologies

¹Corresponding author.

Contents

1	Introduction	1
2	Dispersion suppression with FFAG magnets	2
3	Simulation set-up	3
4	Fitting method	3
5	Results	5
6	Positional errors	6
7	Discussion of the effects of positional errors	8
8	Conclusion	10

1 Introduction

There has recently been a resurgence of interest in Fixed Field Alternating Gradient (FFAG) accelerators [1, 2] and a number of such accelerators have been designed, built or are being developed for various applications including: proton drivers for the Neutrino Factory and spallation neutron sources; accelerator driven sub-critical nuclear reactors; and charged particle therapy [3–7]. The fixed fields used in such accelerators naturally lead to a momentum dependence in the equilibrium position of the beam. A useful addition to such accelerators would be FFAG dispersion suppression. This could lead to the introduction of dispersion-free straights and other applications including, for example, the delivery of an FFAG beam into a rotating gantry for charged particle therapy [3]. There has been work on FFAG dispersion suppressors for rings [8] and straight transport lines [9]. This paper suggests that a way of improving the momentum range of FFAG dispersion suppressors is to manipulate the multipole components of the FFAG field to compensate for the effects of chromatic aberration terms that become significant over a larger momentum range.

In conventional ‘scaling’ FFAGs, the tunes are kept constant throughout acceleration by using a field profile designed to keep the effective gradient:

$$k_e = \frac{1}{B\rho} \frac{dB_z}{dr} \quad (1.1)$$

constant for all energies, where $B\rho$ is the rigidity, r is the radial position and B_z is the strength of the field perpendicular to r . The dispersion created by the field is such that, as the radial position of a particle increases with increasing momentum, there is a commensurate increase in the field

gradient. This is called the scaling law, and a mid-plane field profile in which this is achieved is described by [1]:

$$B_z(r, \theta) = B_{z0} \left(\frac{r}{r_0} \right)^k F(\theta) \quad (1.2)$$

where k is known as the field index, the subscript zero denotes a reference value and $F(\theta)$ is a periodic function around the ring.

This equation is designed for FFAGs with sector shaped magnets, however, this paper considers rectangular magnets. To create fields suitable for rectangular magnets equation (1.2) is modified to [9]:

$$B_z(x, y) = B_{z0} \left(\frac{y_0 + y}{y_0} \right)^k F(x) \quad (1.3)$$

where x, y and z are Cartesian coordinates, with x longitudinal, y horizontal and z vertical. The reference position y_0 is the radius of curvature of the field multiplied by a large factor and y is the horizontal position measured from that point. Setting $y_0 \gg y$ ensures that the field lines are effectively straight and parallel. This can be separated into multipole components using a Taylor expansion:

$$B_{z0} \left(\frac{y_0 + y}{y_0} \right)^k = B_{z0} \left[1 + b_1 \frac{y}{y_0} + b_2 \left(\frac{y}{y_0} \right)^2 \dots + b_n \left(\frac{y}{y_0} \right)^n \right] \quad (1.4)$$

where:

$$b_n = \frac{k \dots (k - (n - 1))}{n!} \quad (1.5)$$

By considering the quadrupole term here, it can be seen that, in order to conserve focusing strength when switching from r_0 to the much larger y_0 , the field index must be multiplied by the same large factor so that $\frac{k}{y_0}$ is kept constant. (From now on $\frac{k}{y_0}$ is referred to simply as k). This modification to the scaling law can be applied to a straight transport line [9], but can also be used for circular accelerator designs [10].

The built-in dispersion of FFAGs creates a problem when low dispersion points are required in a lattice. This paper builds on previous work [3, 9, 11, 12] to show how high-order dispersion suppression can be achieved with FFAG magnets in which the scaling law has been broken.

2 Dispersion suppression with FFAG magnets

The technique for FFAG dispersion suppression is similar to simple FODO dispersion suppression, but with an important difference. Horizontal dispersion is excited by dipole fields and focused by horizontally-focusing quadrupole fields. In a simple periodic FODO lattice, split into ‘normal’ and ‘suppression’ sections, dispersion and its derivative can be brought to zero if: the suppression section has an $n\pi$ phase advance (where $n = 1, 3, \dots$); the derivative of dispersion is zero at the interface of the two sections; the lattice is periodic; and the bend angle of the suppression section is half that of the normal section [13, p.63]. Halving the bending strengths allows the quadrupoles to focus the dispersion.

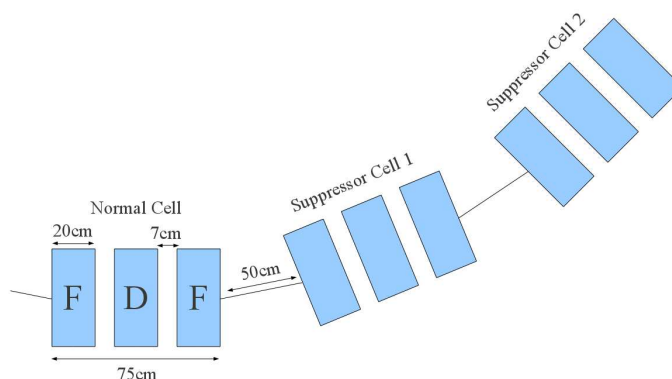


Figure 1. Schematic of the cell lay-out for the suppressor. There is 22.5° bending in each cell.

With FFAG dispersion suppression, the dipole fields are kept constant, and instead, the strength of the quadrupole focusing component of the field is doubled. By inspecting equation (1.4) one can see that this can be achieved by doubling the field index k .

FFAG dispersion suppression has been discussed in ref. [9], where it is noted that it is only useful over a limited energy range. This is because of chromatic aberration which, to the first order, increases with fractional deviation of momentum from the reference orbit and k_e (equation (1.1)). Higher order chromatic aberration includes fringe fields, the effects of dispersion functions and other terms [14, p.172]. This is a general problem for all dispersion suppressors, however, the multipole components that define the field in the FFAG magnets can be varied to empirically compensate for the chromatic aberration and so reduce the residual dispersion.

3 Simulation set-up

This study uses triplet cells of rectangular magnets in a focusing-defocussing-focusing (FDF) configuration. An FFAG defocussing field has a negative sign, which not only means negative focusing, but also negative bending. Figure 1 is a schematic of the three cells forming a dispersion suppressor which were simulated using the particle tracking code Zgoubi [15]. The two ‘Suppressor Cells’ are designed with $\frac{\pi}{2}$ phase advances and k values double that in the ‘Normal Cell’. The momentum range considered is the clinically useful range for proton therapy [3, p.5]: $0.369 \rightarrow 0.729$ GeV/c.

Figure 2 shows the tracks through one normal cell and two suppressor cells of particles with five different momenta covering the entire energy range; figure 3 shows how the final position depends on the momentum of the particle and figure 4 shows the final deflection.

4 Fitting method

For simplicity during the fitting process, the dispersion suppressor was considered in reverse; i.e. the particles were started with zero horizontal position and angle at the end of suppressor cell 2 in figure 1 and passed through suppressor cell 1 into the normal cell. The displacements of the equilibrium orbits away from the reference orbit in figure 2 must be corrected to improve the dispersion suppression.

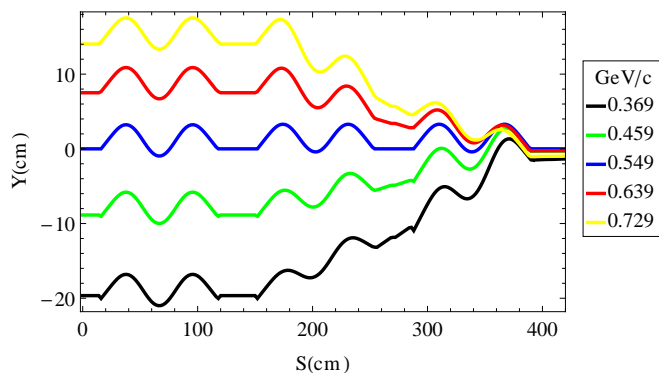


Figure 2. Tracks through a scaling dispersion suppressor for five different momenta. Significant dispersion is visible at around 400cm.

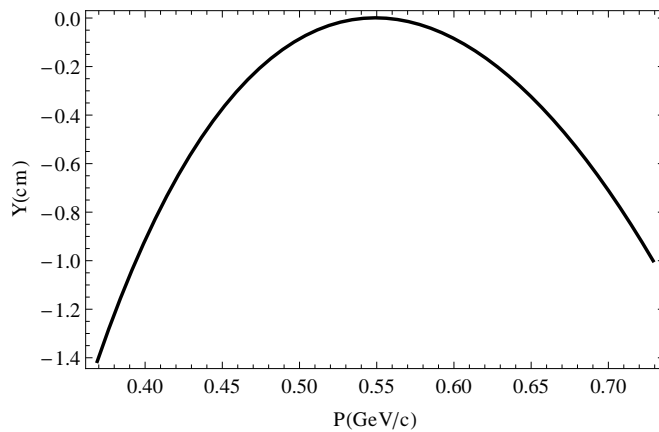


Figure 3. Horizontal position vs momentum at the end of a scaling dispersion suppressor.

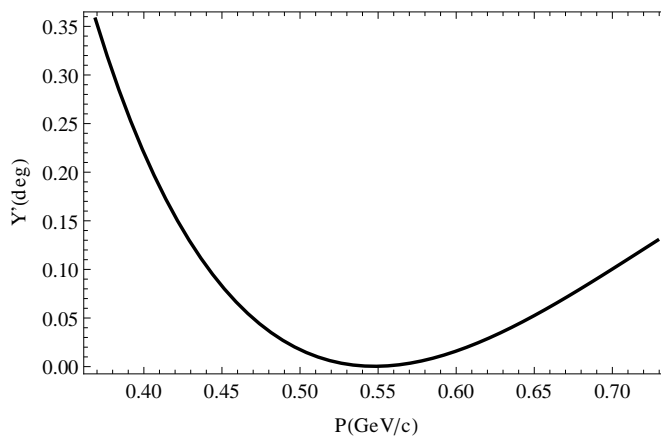


Figure 4. Horizontal deflection vs momentum at the end of a scaling dispersion suppressor.

Using the Taylor expansion in equation (1.4) means the individual multipole components can

be varied to control the shape of the field profile and empirically compensate for the effect of the chromatic aberrations (a similar approach has been used here [16] to solve a related problem). Truncating the series at the decapole term ($n = 4$) was found to give enough variables in the three cells to create the required field shapes.

Although the multipole strengths can be varied in all three cells, the amount of overlap of particle tracks in the suppressor cells (particularly suppressor cell 2) makes them less useful for fitting. For this reason, it is easier to fit the equilibrium orbits in the normal cell to the positions of the particles as they exit the suppressor cells than vice versa.

The following multi-step fitting procedure was found to produce the best results. In the first step, the multipole values in the suppressor cells are varied to ensure the phase advance across the momentum range is as close to π as possible.

With the particles being run through the suppressor cells in reverse, the angles of the particles are fit to zero as they exit suppressor cell 1, ignoring the y position. To avoid the fitting function arriving at a solution with zero field through all magnets, and because of the overlapping particle tracks in cell 2, only cell 1 was varied to fix the angle. The k value of suppressor cell 2, however, can be used to tweak the dispersion in the resulting normal cell. So for example, if the resulting aperture is too large, the k of suppressor cell 2 could be increased to reduce it. This can only be taken so far, however, as varying k has an effect on the phase advance.

In the final step, the multipole components in the normal cell are varied to match the equilibrium orbits to the y positions of the particles as they exit suppressor cell 1.

This is a summary of the procedure:

- (i) Fit the tune of the alignment orbit particle to π through both suppressor cells.
- (ii) Fit the angles of the particles, as they exit the suppressor cells, to zero by varying the field components of suppressor cell 1 only.
- (iii) Fit the equilibrium orbit positions in the normal cell to the exit positions from the suppressor cells (with the particles being run in reverse).

5 Results

The resulting dispersion suppressor restricts the final deviation in horizontal position and angle to within 0.5mm and 0.03° (0.5 mrad), which can be seen in figures 6 and 7. Figure 5 shows the tracks through the modified dispersion suppressor. The values of the constants for equation 1.4 are summarised in table 1.

The square root of the β functions through the dispersion suppressor are shown in figure 8 and the phase advance in figure 9. Because each particle's path through a dispersion suppressor is not along its equilibrium orbit, there is variation in all of the Twiss functions and the phase advance dependent on momentum. This might result in periodic orbits not being available for all momenta because the variation in tune may excite a resonance. Other designs might be able to overcome this problem, but since the design considered here is a single pass lattice, a periodic solution has not been pursued.

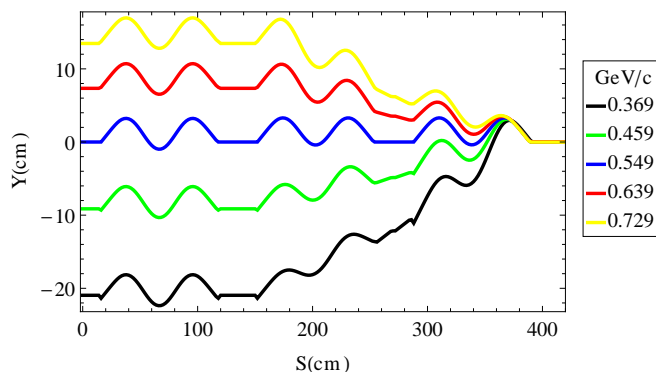


Figure 5. Tracks through a non-scaling FFAG dispersion suppressor with the multipole components varied to create zero dispersion at the end.

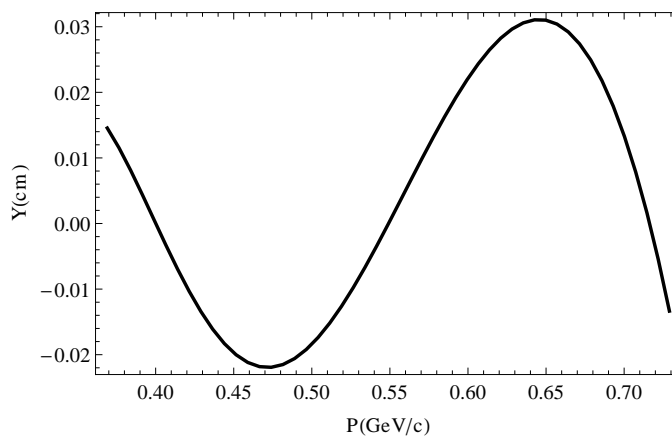


Figure 6. Horizontal position vs momentum at the end of a non-scaling dispersion suppressor. Notice the change in scale from figure 3.

Table 1. Values for the multipole constants (b_n) in equation 1.4 for a non-scaling dispersion suppressor. For all cells, y_0 is set to 10^5 cm.

Cell	Bz_0 (T) [F,D]	b_1 $\times 10^3$	b_2 $\times 10^6$	b_3 $\times 10^9$	b_4 $\times 10^{10}$
Normal Cell	3.39, -4.51	1.907	2.404	2.731	0.115
Suppressor 1	1.26, -3.98	4.143	5.774	23.19	458.9
Suppressor 2	1.32, -4.00	4.003	7.458	8.301	1163

6 Positional errors

To see how positional errors of the magnets may affect the dispersion suppressor, a section of lattice was studied, comprising of four suppressor cells with a dispersion suppression point between the

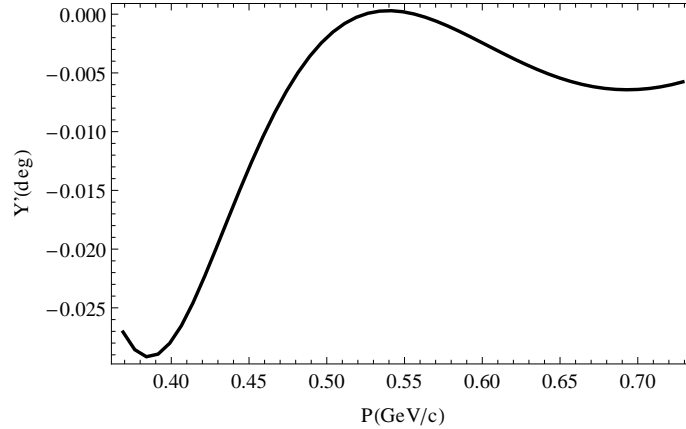


Figure 7. Horizontal deflection vs momentum at the end of a non-scaling dispersion suppressor. Notice the change in scale from figure 4.

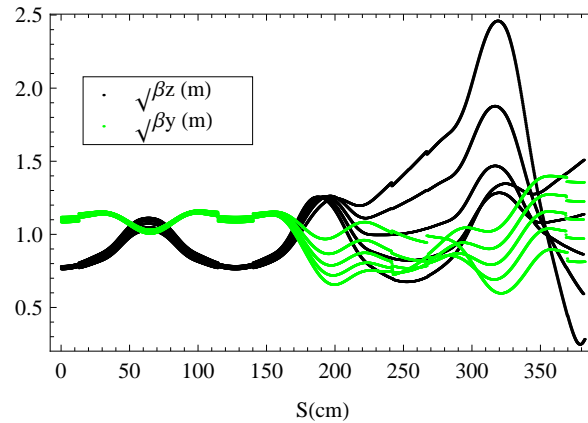


Figure 8. Square root of the beta functions through the non-scaling dispersion suppressor, with initial values those for the normal cell (ignore graph discontinuities).

second and third cells. The particles were started at the y positions of their equilibrium orbits in a ‘normal cell’ and if no errors were present, they would return to those y positions at the end of the lattice.

Vertical, horizontal and longitudinal magnet positioning errors were considered. To simulate random errors, nine error magnitudes were chosen, ranging from $10\mu\text{m}$ to 1cm . These were used as standard deviations on Gaussian distributions with mean values of zero. At every magnitude, a different error pattern was chosen from the distribution, particles at five momenta covering the range $0.369 \rightarrow 0.729$ GeV/c were tracked and their final positions recorded. This was repeated 500 times to improve the statistics.

Plots of the standard deviations of the resulting errors are presented in figures 10, 11, 12 and 13. The first two show the horizontal errors caused by all three types of magnet position error and the latter two show the vertical errors caused by vertical magnet position errors only, as this was the only type of error included in this study to have an effect in the vertical plane. The gradients of the fitted straight lines are known as the the amplification factors and are shown in table 2.

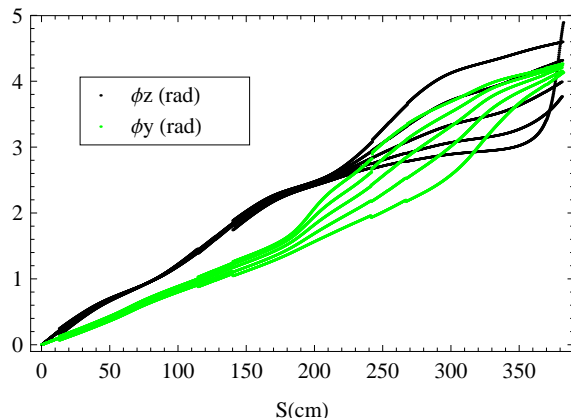


Figure 9. Phase advance through the non-scaling dispersion suppressor. As in figure 8 the discontinuities are artefacts and can be ignored.

Table 2. Amplification factors for all error studies. Key for error types: H = Horizontal, V = Vertical, L = Longitudinal, Pos = Position, Ang = Angle.

Magnet Position	Particle Error	0.369	0.459	0.549	0.639	0.729	
Error Type	Type	(GeV/c)	(GeV/c)	(GeV/c)	(GeV/c)	(GeV/c)	Units
H	H Pos	3.84	3.65	3.49	3.36	3.26	
V	H Pos	0.37	0.38	0.46	0.70	1.03	
V	V Pos	9.93	6.11	4.61	4.01	3.99	
L	H Pos	1.05	1.08	1.02	0.90	0.75	
H	H Ang	2.24	2.10	2.11	2.17	2.26	deg/cm
V	H Ang	0.32	0.21	0.15	0.14	0.20	deg/cm
V	V Ang	4.35	2.97	3.22	4.24	5.71	deg/cm
L	H Ang	1.07	0.73	0.64	0.71	0.83	deg/cm

7 Discussion of the effects of positional errors

The largest amplification factors are those from errors in the vertical plane caused by vertical magnet misalignments. This is due to the behaviour of the vertical betatron function in the dispersion suppressor (see figure 8). A 0.369 GeV/c particle has an almost 10:1 ratio of positional error to magnet misalignment. This means that a realistic alignment accuracy of 50 microns would cause a positional error of around 0.5mm. More importantly, the worst vertical angular error caused by vertical magnet misalignments is approximately 11:2 degrees to cm. A 50 micron misalignment here could cause 0.03° deflection, which would result in a 1.5mm displacement after a 3m drift. Horizontal misalignments of 50 microns would cause a maximum positional displacement of 0.2mm, while the maximum deflection caused would result in a 0.6mm displacement after a 3m drift. The longitudinal misalignments are the least important of the types studied, with the deflection caused creating a 0.3mm displacement after a 3m drift.

For comparison, the target positioning error found acceptable for the scanning system of a

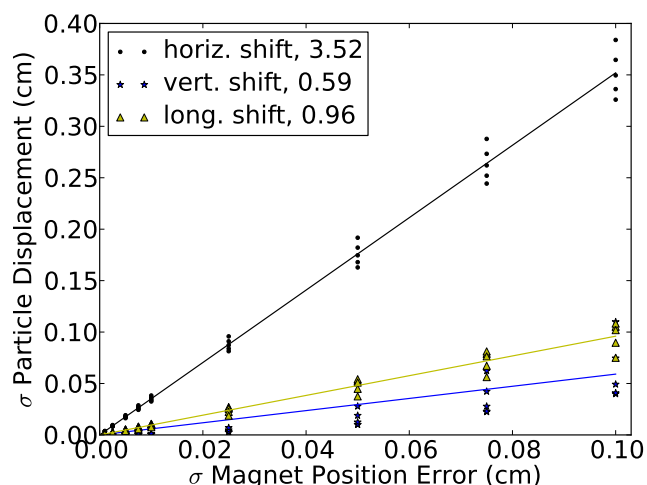


Figure 10. Sensitivity of horizontal particle position to errors in the magnet positions in an FFAG dispersion suppressor. The effect of three types of magnet position error are shown: horizontal, vertical and longitudinal. Errors were simulated for five momenta in the range $0.369 \rightarrow 0.729$ GeV/c at each magnet error magnitude, however for clarity, lines were fitted to the averages and the amplification factors shown in the legend are the gradients of those lines. Individual amplification factors can be found in table 2. The magnet misalignments have a Gaussian distribution and the standard deviations of the resulting positional errors are shown.

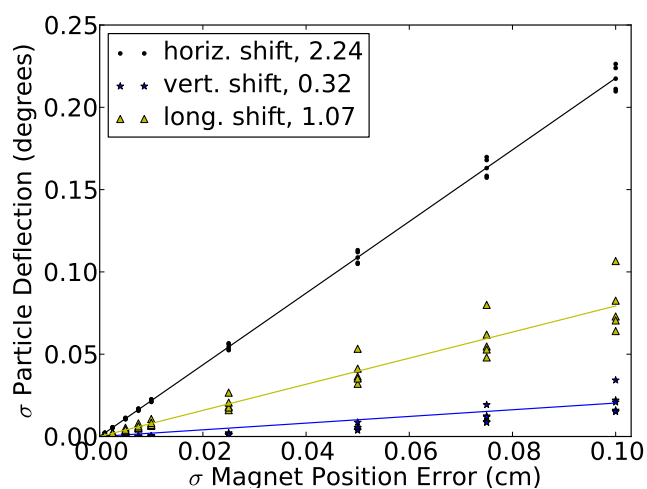


Figure 11. Sensitivity of horizontal particle deflection to errors in the magnet positions in an FFAG dispersion suppressor. The effect of three types of magnet position error are shown: horizontal, vertical and longitudinal. Errors were simulated for five momenta in the range $0.369 \rightarrow 0.729$ GeV/c at each magnet error magnitude, however for clarity, lines were fitted to the averages and the amplification factors shown in the legend are the gradients of those lines. Individual amplification factors can be found in table 2.

proton therapy complex is 0.3mm [3, p.12], so an error of 1.5mm would have to be compensated.

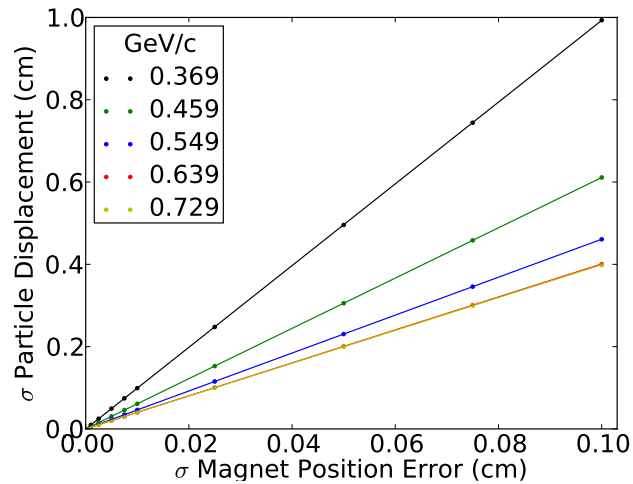


Figure 12. Sensitivity of vertical particle position to vertical errors in the magnet positions in an FFAG dispersion suppressor. Errors were simulated for five momenta, shown in the legend, and amplification factors can be found in table 2.

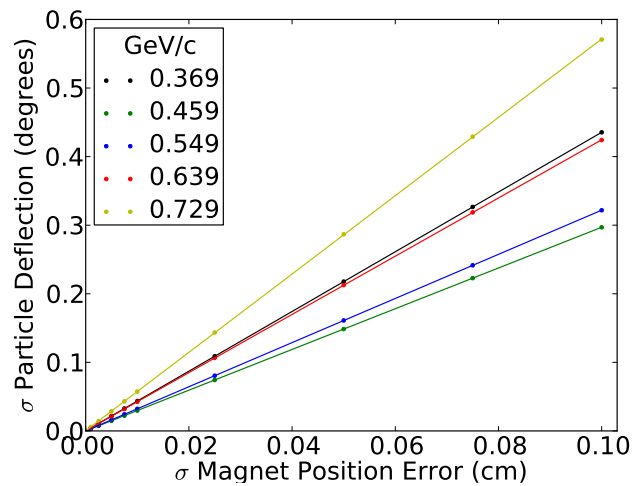


Figure 13. Sensitivity of vertical particle deflection to vertical errors in the magnet positions in an FFAG dispersion suppressor. Errors were simulated for five momenta, shown in the legend, and amplification factors can be found in table 2.

8 Conclusion

High-order dispersion suppression for FFAG optics has been achieved in a simulation of a three cell lattice by compensating for the effects of chromatic aberration using the multipole components of the fields in the suppressor cells and the normal cell. This process successfully increased the momentum range of an FFAG dispersion suppressor to the clinically useful range for proton therapy [3, p.5]. The price paid for this is the possible loss of periodicity of some of the beta functions (see figure 8). Sensitivity to random errors in horizontal, vertical and longitudinal magnet positions

have been explored and it was found to be comparable to positioning errors found acceptable for the scanning system of a proton therapy complex [3]. Sensitivity was greatest in the vertical plane and it was found that a 50 micron alignment accuracy could cause around a 0.5mm positional error and a 0.03° deflection. This could be reduced by further optimising the vertical betatron function.

References

- [1] K.R. Symon, D.W. Kerst, L.W. Jones, L.J. Laslett and K.M. Terwilliger, *Fixed-field alternating-gradient particle accelerators*, *Phys. Rev.* **103** (1956) 1837.
- [2] M. Craddock, *The rebirth of the FFAG*, *CERN Courier* (2004).
- [3] K. Peach et al., *PAMELA design report*, CONFORM (2011).
- [4] Y. Kuriyama et al., *Beam study of FFAG accelerator at KURRI*, in proceedings of *IPAC10*, Kyoto, Japan (2010).
- [5] F. Meot, *The RACCAM FFAG project*, in proceedings of *NuFact 07*, Okayama, Japan (2007).
- [6] C. Johnstone, W. Wan and A. Garren, *Fixed field circular accelerator designs*, in proceedings of *PAC99*, New York, USA (1999).
- [7] C.R. Prior, *Neutrino factory proton driver: preferred scenarios and remaining issues*, *PoS(Nufact08)070*, in proceedings of *10th international workshop on neutrino factories, super beams and beta beams*, Valencia, Spain (2008).
- [8] J.B. Lagrange, T. Planche and Y. Mori, *Scaling FFAG accelerator for muon acceleration*, in proceedings of *NuFact 10*, Mumbai, India (2010).
- [9] S. Machida and R. Fenning, *Beam transport line with scaling fixed field alternating gradient type magnets*, *Phys. Rev. ST Accel. Beams* **13** (2010) 084001.
- [10] S.L. Sheehy, K. Peach, H. Witte, D. Kelliher and S. Machida, *Fixed field alternating gradient accelerator with small orbit shift and tune excursion*, *Phys. Rev. ST Accel. Beams* **13** (2010) 040101.
- [11] R. Fenning, S. Machida, D. Kelliher, A. Khan and R. Edgecock, *A non-scaling FFAG gantry design for the PAMELA project*, in proceedings of *IPAC10*, Kyoto, Japan (2010).
- [12] R. Fenning, *Novel FFAG gantry and transport line designs for charged particle therapy*, Ph.D. Thesis, School of engineering and design, Brunel University, (2011).
- [13] B.J. Holzer, *Lattice design in high-energy particle accelerators*, in proceedings of *CERN accelerator school 10*, DESY, Hamburg, Germany (2003).
- [14] S.Y. Lee, *Accelerator physics*, World Scientific, Singapore (1999).
- [15] F. Meot and S. Valero, *Zgoubi user's guide*, edition 4.3 (2008).
- [16] P. Snopok, *Optimisation of accelerator parameters using normal form methods on high-order transfer maps*, Michigan State University, Ph.D. Thesis (2007).